Compton scatter profiles for warm dense matter

S. Sahoo, G. F. Gribakin, G. Shabbir Naz, J. Kohanoff, and D. Riley*
School of Mathematics and Physics, The Queen's University of Belfast, Belfast BT7 1NN, United Kingdom
(Received 23 October 2007; published 2 April 2008)

In this paper, we discuss the possibility of using x-ray Compton scattering as a probe of the outer electronic structure of ions immersed in warm dense matter. It is proposed that the x-ray free-electron lasers currently under construction will provide an ideal tool for this, with the main pulse being used to create a uniform well-defined sample and the third harmonic providing a clean monochromatic probe. We model the plasma photon scatter spectrum by combining self-consistent finite-temperature electronic structure calculations with molecular dynamics simulations of the ion-ion structure factor. In particular, we present bound-free Compton profiles that are more accurate that those obtained using form factor or impulse approximations.

DOI: 10.1103/PhysRevE.77.046402 PACS number(s): 52.25.Os, 52.27.Gr

I. INTRODUCTION

The study of warm dense matter (WDM) is currently of wide interest due to its application to astrophysical and planetary sciences and to fusion science [1,2]. It is also of intrinsic scientific interest as the parameter regime it covers (with densities of 10^{-2}–10^{1} g cm^{-3} and temperatures of 1–100 eV) is not well understood, by either solid state physics or classical plasma theory. Experimentally, one of the major challenges is the creation of a sample that is both spatially uniform in density and temperature and long lived enough to be probed with some technique such as x-ray absorption spectroscopy, radiography, or x-ray scatter.

In this paper we are proposing an experiment where an intense x-ray free-electron laser (XFEL) is used to create a uniform sample and its third harmonic is used as an x-ray scatter probe. The duration of this probe is much shorter than the timescale for hydrodynamic expansion of the sample created, thus allowing a well defined temperature and density to be probed.

Of special interest is the electronic structure of ions in dense plasmas. The outer electrons, in particular, are severely perturbed by the presence of the plasma environment. One method for investigating the electronic structure is x-ray Compton scattering. This is a technique that has been used in solid-state physics [3,4] and is a probe of the electron momentum distribution. By Fourier transforming the result we can, in principle, recover the spatially dependent electronic wave function.

Such an experiment, as in other WDM experiments, would require the generation of a uniform, well-defined warm dense matter sample and the availability of an intense quasimonochromatic x-ray source. Both of these requirements are met by the x-ray free-electron lasers currently under construction [5–7]. One of the beamlines (SASE 3) at the DESY XFEL will generate 100 fs pulses of 2×10^{13} photons per pulse at 3.1 keV photon energy in a beam 60–70 μm in diameter. We propose to use this beam as a creator of solid-density foils with temperatures of up to 10 eV. We then propose that the third harmonic beam (2×10^{11} photons per pulse) can be used as the scatter source. A principal reason for using the third harmonic, rather than splitting the fundamental into two beams, is that it allows us to probe soon after plasma creation without the need to temporally resolve the plasma creation and probing beams. The scatter spectrum will consist of three basic components. There will be an unshifted peak due to coherent Rayleigh scatter from the strongly bound electrons (i.e., those whose binding energy is greater than the free-electron Compton shift for the particular scattering angle). There will also be a free-electron scatter feature and, finally, there are Compton scatter profiles originating from bound electrons which reflect the momentum distribution of the bound states.

Spectrally resolved x-ray scatter from dense plasmas has been investigated experimentally [8,9] and theoretically [10–12] using an approach similar to that used for liquid metals [13]. Although attention has been paid to the validity of different approximations for the free-electron feature [12] and for the ion-ion structure factor [14], less work has been directed to the bound-free Compton profiles. Previously, the results of theory developed for isolated atoms [15–18] have been applied, with the shells included being dependent on the degree of ionization calculated for the plasma conditions in question. In this paper we take a different approach, in that we use a self-consistent field (SCF) approach to calculate the electronic structure with boundary conditions set for an atom immersed in a plasma environment [19]. We believe that this is the first time the Compton profiles have been calculated for a dense plasma as opposed to isolated ions or condensed matter. It is worth pointing out that similar calculations applied to the study of optical properties of plasmas [20] have been made, based on the average-atom model. The details of our simulation are outlined below.

II. SIMULATION METHODS

Following Ref. [21], we describe scattering from aluminum plasma containing N ions per unit volume. We choose aluminum because it is a convenient material to work with experimentally and for this reason it has been widely studied in warm dense matter physics. We denote the nuclear charge of the ion Z and the total number of electrons (bound +free) per unit volume is NZ. We probe this system with x rays of frequency ω_0 such that $\hbar\omega_0 \gg E_I$, the ionization potential of any bound electron. During this process, the inci-

*d.riley@qub.ac.uk

dent photon transfers momentum $\hbar\mathbf{k}$ and energy $\hbar\omega=\hbar\omega_0-\hbar\omega_1$, where $\hbar\omega_1$ is the energy of scattered photons. In the nonrelativistic limit

$$k=|\mathbf{k}|=\frac{4\pi}{\lambda_0}\sin(\theta/2), \tag{1}$$

where $\lambda_0=2\pi c/\omega_0$ is the probe wavelength, and θ is the scattering angle. Following the approach of Chihara [13], the scattering cross section can be written in terms of the dynamical structure factor $S(k,\omega)$ of all the electrons in the plasma as

$$S(k,\omega)=|f_I(k)+q(k)|^2S_{ii}(k,\omega)+Z_fS^0_{ee}(k,\omega)+Z_b\int S_{be}(k,\omega-\omega')S_s(k,\omega')d\omega', \tag{2}$$

where Z_f and Z_b are the number of free and (tightly or weakly) bound electrons, respectively. The first term in Eq. (2) describes the density correlations that dynamically follow the motion of the ion which includes the ionic form factor $f_I(k)$, the screening cloud of free electrons $q(k)$, and the ion-ion structure factor $S_{ii}(k,\omega)$. The second term accounts for the contribution from the free electrons with $S^0_{ee}(k,\omega)$, the high-energy part of the electron-electron correlation function [22]. Inelastic scattering by bound electrons is described by the last term of the equation, with $S_{be}(k,\omega)$, the structure factor for bound-free transition modulated by the random thermal motion of the ions, represented by $S_s(k,\omega')$. This last function is approximated by a δ function since none of the proposed experiments will resolve the ion motion.

Although, for completeness, we calculate all terms, the calculation of the bound-free part is the main issue in the present paper. The following section describes the methods we used to calculate the contributions of different terms to the total dynamic structure factor.

A. Electronic structure of plasma: Quantum mechanical model

To describe the electronic structure of ions immersed in plasma, we divide the plasma into neutral cells, each containing Z electrons, centered on a nucleus of charge Z. The radius of each cell is taken to be the Wigner-Seitz (WS) radius (R) that can be determined from the density and the atomic weight. Implicit in this model is the assumption of spherical symmetry and thus that the solid has melted into a dense plasma state at the time of probing. We can note, in this respect, that Mazevet *et al.* [23] have found in molecular dynamics simulations that, for modest heating of Au, it can take of the order of picoseconds for the initial face-centered cubic structure to disappear. Our ions are lighter and we assume, for now, equal ion and electron temperatures. Nevertheless, this is an issue that we discuss further, below.

Each electron's orbital is assumed to satisfy the self-consistent radial central field Schrödinger equation (in atomic units)

$$\left(-\frac{1}{2}\frac{d^2}{dr^2}-\frac{Z}{r}+\frac{l(l+1)}{2r^2}+V(r)\right)P_{n(\epsilon)l}(r)=\epsilon_{n(\epsilon)l}P_{n(\epsilon)l}(r), \tag{3}$$

with the following set of boundary conditions:

$$P_{n(\epsilon)l}(0)=\left.\frac{dP_{n(\epsilon)l}}{dr}\right|_{r=R}=0,$$

where $P_{n(\epsilon)l}(r)$ is the radial wave function, n (ϵ) denotes bound (continuum) states, and l is the orbital angular momentum quantum number. We expand $P_{n(\epsilon)l}(r)$ in terms of a B-spline basis (as, e.g., in Ref. [24]),

$$P_{n(\epsilon)l}(r)=\sum_i C^i_{n(\epsilon)l}B^\kappa_i(r), \tag{4}$$

where $B^\kappa_i(r)$ are κth-order B-spline functions and $C^i_{n(\epsilon)l}$ are the coefficients determined by diagonalizing the operator in Eq. (3). By using B splines we actually discretize the positive-energy electron continuum.

The potential $V(r)$ inside the cell is the sum of the direct $V_d(r)$ and exchange potential $V_{\rm ex}(r)$. The direct part of the potential is obtained from

$$\nabla^2V_d(r)=4\pi\rho, \tag{5}$$

where the electron density $\rho=\rho_b+\rho_f$ contains the contributions from both bound and free (i.e., continuum state) electrons. We replace the exact exchange potential with Slater's approximate local exchange potential [25],

$$V_{\rm ex}(r)=-\frac{3}{2}\left(\frac{3}{\pi}\rho(r)\right)^{1/3}. \tag{6}$$

The bound state contribution to the total density is

$$\rho_b=\frac{1}{4\pi r^2}\sum_{nl}2(2l+1)f_{nl}P^2_{nl}, \tag{7}$$

where $f_{nl}=\{1+\exp[(\epsilon_{nl}-\mu)/kT_e]\}^{-1}$ is the Fermi statistical occupancy for an orbital with quantum numbers n,l, μ is the chemical potential, and T_e is the electronic temperature. The contribution from the continuum states ρ_f is given by the same formula with the bound state radial wave function $P_{nl}(r)$ replaced by the continuum wave function $P_{\epsilon l}(r)$ [24].

The chemical potential μ is obtained from the neutrality of the Wigner-Seitz cell,

$$Z=\int_0^R 4\pi r^2\rho(r)dr. \tag{8}$$

The electrostatic potential $V(r)$, the chemical potential μ, and the electron density $\rho(r)$ and hence the radial wave functions $P_{n(\epsilon)l}$ are obtained by self-consistently solving Eqs. (3)–(8). We apply this model in the present calculation. We considered aluminum (Al) at metallic density (2.7 g cm^{-3}) and three different temperatures. The corresponding WS radius is $R=2.99$ a.u. The potential in these cases supports four bound states $(1s,2s,2p,3s)$. Table I shows the state energies, occupation numbers, and the numbers of bound and free electrons, Z_b and Z_f.

TABLE I. Electronic structure of Al at $\rho=2.7$ g cm^{-3}.

States	Energies (a.u.) and occupation numbers					
	$T_e=2$ eV		$T_e=5$ eV		$T_e=10$ eV	
$1s$	−54.84	2.00	−54.87	2.00	−54.94	2.00
$2s$	−3.65	2.00	−3.67	2.00	−3.72	1.99
$2p$	−2.28	6.00	−2.30	5.99	−2.35	5.96
$3s$	−0.21	1.75	−0.22	1.09	−0.23	0.65
Z_b		11.75		11.09		10.62
Z_f		1.25		1.91		2.38

It is interesting to note that the model predicts a finite occupancy of the M shell ($3s$), in contrast, for example, to the Thomas-Fermi model (with no shell effects) which predicts average ionization greater than 3. The nature of the $3s$ orbital, however, is that, although it is energetically bound, it is delocalized and has a significant amplitude at the cell edge. In this respect, it is known that there is not always a sharp distinction between free and bound electrons in a dense plasma [26].

B. Calculation of $f_I(k)$ and $q(k)$

Using the bound state density $\rho_b(r)$ obtained self-consistently, we estimated $f_I(k)$ which governs the amount of scattering utilizing the following expression:

$$f_I(k) = \int_0^R 4\pi r^2 \rho_b(r) \frac{\sin kr}{kr} dr, \tag{9}$$

and the screening cloud of free electrons is given by [13]

$$q(k) = \sqrt{Z_f} \frac{S_{ei}(k)}{S_{ii}(k)}, \tag{10}$$

where $S_{ei}(k)$ and $S_{ii}(k)$ are the electron-ion and ion-ion static structure factors respectively. $S_{ei}(k)$ is related to the electron-electron and ion-ion structure factors [27].

C. Calculation of $S_{ii}(\boldsymbol{k},\omega)$

To determine the ion-ion structure factor $S_{ii}(k,\omega) \sim S_{ii}(k)$ (for large ω), we performed a molecular dynamics study which is based on the embedded atom model [28]. The simulations are carried out in a cubic cell of $N_{\rm at}=256$ atoms. Periodic boundary conditions are used to simulate bulk geometry. The equation of motion are solved using velocity-Verlet algorithm with a time step of 1 fs. From the density correlation $\rho_i(\mathbf{k}) = \sum_{i=1}^{N_{\rm at}} e^{i\mathbf{k}\cdot\mathbf{r}_i}$, we calculate the structure factor as

$$S_{ii}(k) = \frac{1}{N_{\rm at}} \langle \rho(\mathbf{k}) \rho(-\mathbf{k}) \rangle = \frac{1}{N_{\rm at}} \left\langle \sum_{i,j=1}^{N_{\rm at}} e^{i\mathbf{k}\cdot(\mathbf{r}_i - \mathbf{r}_j)} \right\rangle, \tag{11}$$

where $\mathbf{r}_i$ are the atomic coordinates.

D. Calculation of $S_{ee}(\boldsymbol{k},\omega)$

The second term of Eq. (2) accounts for the free-electron density-density correlations and can formally be obtained from the fluctuation dissipation theorem [29]

$$S_{ee}^0(k,\omega) = -\frac{\hbar}{1-\exp(\hbar\omega/k_B T_e)} \frac{\epsilon_0 k^2}{\pi e^2 n_e} \mathrm{Im}\left(\frac{1}{\epsilon(k,\omega)}\right), \tag{12}$$

where $\epsilon(k,\omega)$ is the electron dielectric response function and the remaining variables have the usual meanings.

The dielectric response function $\epsilon(k,\omega)$ in Eq. (12) can be calculated using the random phase approximation (RPA). This approximation assumes the interparticle interactions are weak so that the nonlinear interactions between density fluctuations can be neglected [30].

In conditions such as those where collisions in the plasma become important and the RPA is not valid, we can include collisions by use of local field corrections as described by Gregori *et al.* [11] or by use of the Mermin ansatz as described by Redmer *et al.* [31].

Figure 1(a) shows the comparison of the RPA with static local field corrections (SLFCs) and dynamic local field corrections (DLFCs), as in Ref. [11] for the free-electron dynamic structure factor of an aluminum plasma in backscatter geometry. Clearly, collisions are not very important in backscatter, and we can treat the free-electron part only using the RPA. In contrast, for forward scatter in Fig. 1(b) the collisions make a difference. The parameter $\omega_{pe}=(e^2 n_e/\epsilon_0 m_e)^{1/2}$ in Fig. 1 is the electron plasma frequency, where n_e is the electron density and m_e is the electron mass. In the full scatter cross-section calculations presented below, we will use the DLFC simulations to represent the free-electron contribution.

E. Calculation of bound-free transitions

In the nonrelativistic approximation, the differential photon scattering cross section by an atomic system can be obtained by taking the lowest-order matrix element of $\mathbf{A}^2$ [32] in the Hamiltonian, and summing over all possible electronic transitions $i \to f$, which gives

$$\frac{d\sigma}{d\Omega_1 d\omega_1} = \left(\frac{d\sigma}{d\Omega_1}\right)_{\rm Th} \left(\frac{\omega_1}{\omega_0}\right) \sum_{i,f} |M_{fi}|^2 \delta(\epsilon_f - \epsilon_i - \omega), \tag{13}$$

where

$$M_{fi} = \langle f | e^{i\mathbf{k}\cdot\mathbf{r}} | i \rangle, \tag{14}$$

and $\omega_1 = \omega_0 + \epsilon_i - \epsilon_f$ is the energy of the scattered photon, ϵ_i and ϵ_f being the initial and final state energies, $(d\sigma/d\Omega_1)_{\rm Th}$ is

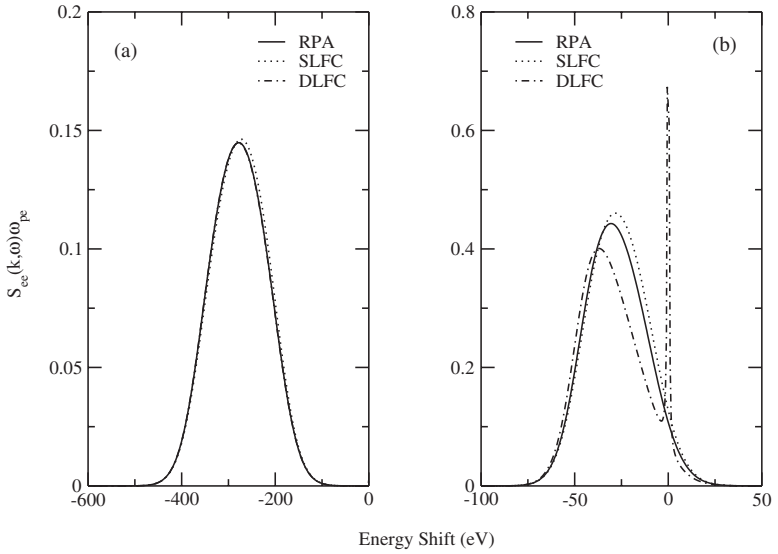

FIG. 1. Comparison of RPA with SLFC and DLFC results for aluminum plasma with density $\rho=2.7$ g cm^{-3}, probe energy $\hbar\omega_0=9.3$ keV, electron temperature $T_e=5$ eV, electron density $n_e=1.15\times10^{23}$ cm^{-3}: scattering angle θ = (a) 130° and (b) 30°.

the Thomson scattering cross section, and i and f are the initial (bound) and final (continuum) electron states in Al under various plasma conditions obtained as outlined in Sec. II A.

The cross section (13) is related to the structure factor $S_{be}(k,\omega_1)$,

$$\frac{d\sigma}{d\Omega_1 d\omega_1}=\left(\frac{d\sigma}{d\Omega_1}\right)_{\mathrm{Th}}\left(\frac{\omega_1}{\omega_0}\right)S_{be}(k,\omega_1). \tag{15}$$

In the present calculation we use a representation of the continuum by means of spline-based discrete states. We obtain the structure factor as a continuous function of frequency as

$$S_{be}(k,\omega_1)=\sum_{i,f}|\langle f|e^{i\mathbf{k}\cdot\mathbf{r}}|i\rangle|^2\tilde{\delta}(\epsilon_f+\omega_1-\epsilon_i-\omega_0), \tag{16}$$

where $\tilde{\delta}(\varepsilon)=(2\pi\Delta_f^2)^{-1/2}\exp[-\varepsilon^2/(2\Delta_f^2)]$ is a Gaussian finite-width "δ function." We take their widths Δ_f to be equal to half of the energy differences between neighboring positive energies ϵ_f.

III. RESULTS

Figure 2 shows the contributions from different subshells of Al to the bound-free structure factor calculated using the procedures discussed in the preceding section. We consider four density cases; isolated atoms, a low-density plasma at 0.01 g cm^{-3}, solid density (2.7 g cm^{-3}), and a compressed case (5.4 g cm^{-3}). In all cases the temperature is 5 eV, the scatter angle is 130°, and the probe photon energy is 9.3 keV. In order to better see the effect of the plasma environment, the data are presented as the dynamic structure factor *per electron* rather than per atom, as the occupation numbers of the shells will also change with density. We can see two principal points from this data. First, it is clear that there is a contribution from the M shell which has orbitals with a finite occupation probability. This contribution would be missing from calculations in which, for example, the Thomas-Fermi (TF) model was used, since the average ionization would be greater than 3 and it would be taken that the M shell is empty. The second point is that the shape of the Compton profile changes with density. This could be expected from the fact that the wave functions are affected by the plasma environment. It is precisely this sort of effect on atomic physics that is at the heart of the science of WDM, and we believe this illustrates the potential value of spectrally resolved x-ray scatter measurements in the experimental investigation of WDM.

As mentioned in Sec. I, we believe that the forthcoming XFEL facilities are a good testbed for WDM. This XFEL will be capable of rapidly heating solid density foils to temperatures in the WDM regime (>1 eV). Thus, in the calculations below, we concentrate on the solid density case, varying the temperature and the scatter angle.

Figure 3 presents the calculations of the bound-free Compton profiles for the L and M shells at 30°, normalized by the plasma frequency for a series of temperatures, up to 10 eV, at solid density. These conditions are well within the bounds of what can be created by proposed XFEL heating of a solid Al foil [33]. We can notice immediately that, for this forward scatter mode, the contribution to the M shell is of comparable magnitude to that of the L shell. Since the binding energy of the M-shell electrons is small (see Table I), we need to expect some bound-free contribution to the scatter cross section in the same spectral region where the free-electron feature is expected, as we shall see below. This may complicate analysis if the plasma conditions are analyzed based on the free-electron feature alone. For the L shell, when the increasing value of ω_p is accounted for, the actual cross section is approximately constant with increasing T_e. The M-shell contribution decreases with increasing T_e due to the smaller occupation numbers.

Figure 4 shows the same calculation for backscatter at 130°. We see now that the M shell contribution is a little less important than that of the L shell but still significant.

In Fig. 5 we present a comparison between the bound-free Compton profiles obtained using different approaches. We compare the results generated using the present self-consistent field approach with calculations using both the

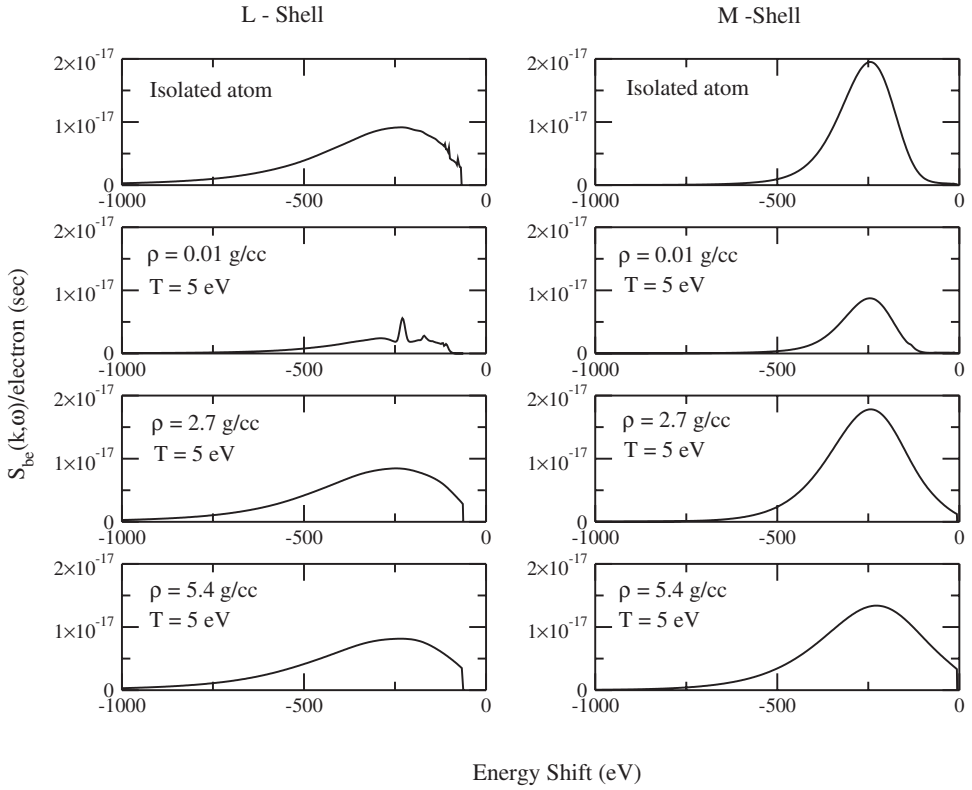

FIG. 2. Contributions of L and M shells of Al to $S_{be}(k,\omega)$ as a function of shift in scatter photon energy for increasing density. The temperature is 5 eV in all cases except the top panel, and the scatter angle is 130°.

impulse approximation (IA) results of Bloch and Mendelsohn [17] and the form factor approximation (FA) of Schumacher *et al.* [18] for the same ionization energy levels and orbital occupation numbers. Both of these methods use hydrogenic wave functions with *effective* nuclear charges. The effective nuclear charges can be derived via binding energies for each orbital or, for example, by requiring that the impulse approximation profile match exact calculations made with a Hartree-Fock code at the center of the profile [16], the former method being used in our comparison here.

We notice that for the L-shell contribution at $\theta=30°$ the IA does not well match the other two calculations. This is easy to understand as the condition for validity of the IA is that $(E_B/E_C)^2 \ll 1$, where E_B is the binding energy and E_C is the Compton energy shift for a free electron. For a scatter angle of 30°, the Compton shift is ~23 eV compared to the L-shell binding energy of ~60–70 eV. For L-shell contributions at 130°, the Compton shift is now ~280 eV and $(E_B/E_C)^2 \ll 1$. We see that all three calculations have similar shapes but the present method shows a higher magnitude due

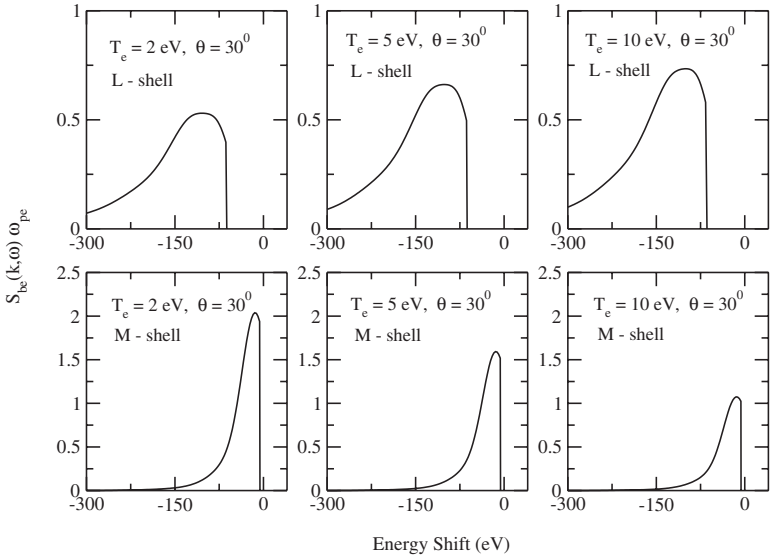

FIG. 3. Compton profile calculations for scatter at 30° with 9.3 keV photons and solid density Al. We see there is a change as the temperature rises from 2 to 10 eV.

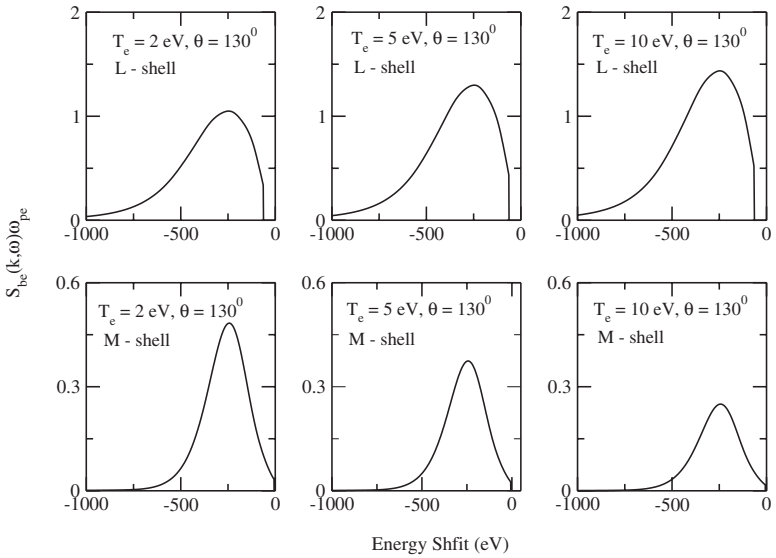

FIG. 4. Compton profile calculations for scatter at 130° with 9.3 keV photons and solid density Al. In this backscatter mode the *M* shell gives a significant contribution.

to the distorted $2p$ wave function. For the *M*-shell cases we expect the IA approximation to be valid and the IA and FA methods are in reasonable accord. However, the *M*-shell wave functions are quite distorted by the plasma environment in the present work, and the resultant contributions are quite different.

Naturally, we wish to see what photon scattering spectra one expects to obtain in an actual experiment. In order to do this we combine the bound and free electron contributions as seen in Fig. 6.

As we can see, for the forward scatter case, there is a dominant contribution from the bound-free profile in the region of the free-electron contribution, and this would need to be considered in the analysis of the scatter spectra of an experiment. At larger angles, we see that the bound-free profile is also a significant part of the experimentally observed spectrum. We can also see that the changing balance between shell contributions means that the profile changes shape with temperature. Thus, fitting of an experimental profile may provide a useful diagnostic of plasma conditions, in particular the temperature, in an XFEL heated target.

In addition to the scatter at 9.3 keV we should be able to detect a scatter spectrum around the 3.1 keV fundamental photon energy. This spectrum would represent scatter during the heating of the target and would be of interest as it may provide some information about the evolution of the plasma from the solid target. In Fig. 7 we can see spectra calculated as above for solid density. As for the 9.3 keV case, the calculations assume equal electron and ion temperatures. We can see that for this photon energy we expect, in the forward scatter mode, to observe plasmon features either side of the Rayleigh peak (seen weakly in the 10 eV case). The ratio of these peaks is governed by the relationship

$$S^0_{ee}(k,-\omega) = S^0_{ee}(k,\omega)\exp(-\hbar\omega/k_B T_e). \tag{17}$$

This relationship is independent of the model used for the free-electron feature and has been proposed as a method of

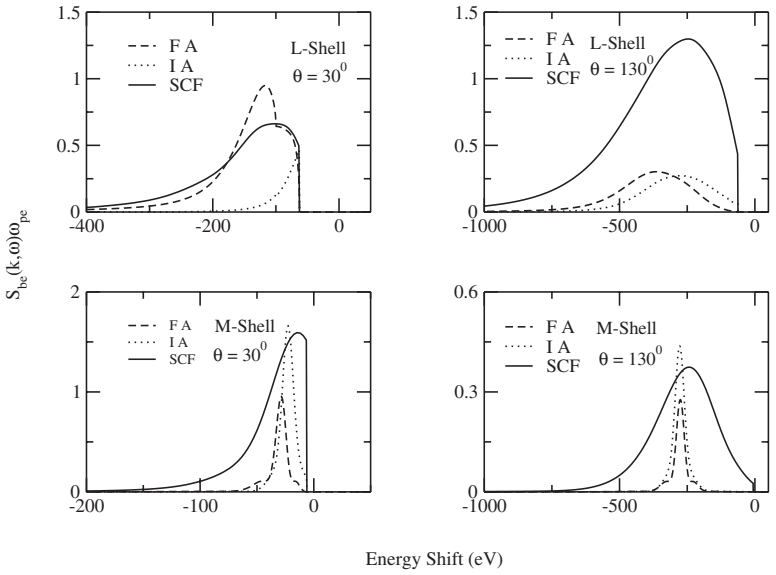

FIG. 5. Bound-free Compton profile calculations for scatter in different approaches: solid line, present method; dashed line, form factor approximation; dotted line, impulse approximation.

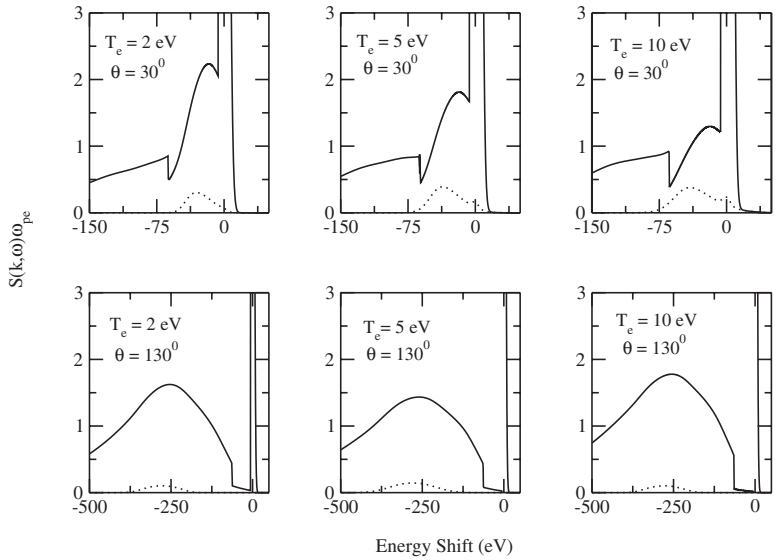

FIG. 6. Expected scatter spectra for 9.3 keV on solid Al target at temperatures 2, 5, and 10 eV. The spectra are folded with a Gaussian instrument width of 0.1% (9.3 eV). The dashed line shows the free-electron contribution.

determining the electron temperature in a warm dense matter sample [9]. For the Al case, it is clear that the contribution of the bound-free Compton profile needs to be considered as well.

We have used Al in this work as it is a commonly used, experimentally practical element. Part of our future work will be to explore the use of other elements to avoid bound-free contributions in the region of the redshifted plasmon feature, so as to allow the red-blue asymmetry to be used as a temperature probe.

IV. EXPERIMENTAL IMPLEMENTATION

In a previous paper [34], we described an experimental arrangement in which the fundamental beam of the SASE3 beamline is separated from the third harmonic by use of a thin silicon nitride grazing-incidence mirror, which reflects the fundamental but efficiently transmits the third harmonic. A further gold mirror is then used to redirect the third harmonic onto the same sample as the fundamental but now with a temporal delay of the order of a picosecond, depending on the mirror separation. As in this work (see Sec. I), a principal point of using the harmonics was to allow distinction between the heating and probing beams with time-integrated diagnostics. The reasons for avoiding time-resolved diagnsotics are that, first; although picosecond resolution is possible with modern streak cameras, the dynamic range for a single shot is very poor (generally significantly less than 10) and jitter associated with integrating many shots significantly reduces available temporal resolution; second, detection efficiency is generally much poorer than in time-integrated diagnostics.

As noted in Ref. [34], the fundamental beam at 3.1 keV is capable of uniformly heating a thin foil of Al to temperatures in excess of 10 eV with easily achievable focusing. The areal atomic density of a 1 μm Al foil is 6×10^{18} cm^{-2}. The cross sections for the bound-free terms, as seen above, vary depending on the angle of scatter and plasma conditions. Typical values from the cases studied indicate that, with 2×10^{11} photons per shot, we can expect $>10^5$ sr^{-1} scattered

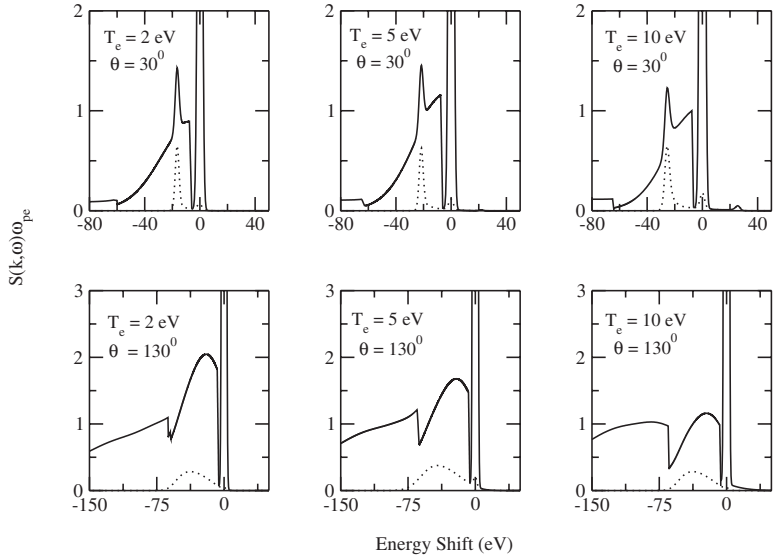

FIG. 7. Expected scatter spectra for 3.1 keV on solid Al target at temperatures 2, 5, and 10 eV. The spectra are folded with a Gaussian instrument width of 0.1% (3.1 eV). The dashed line shows the free-electron contribution.

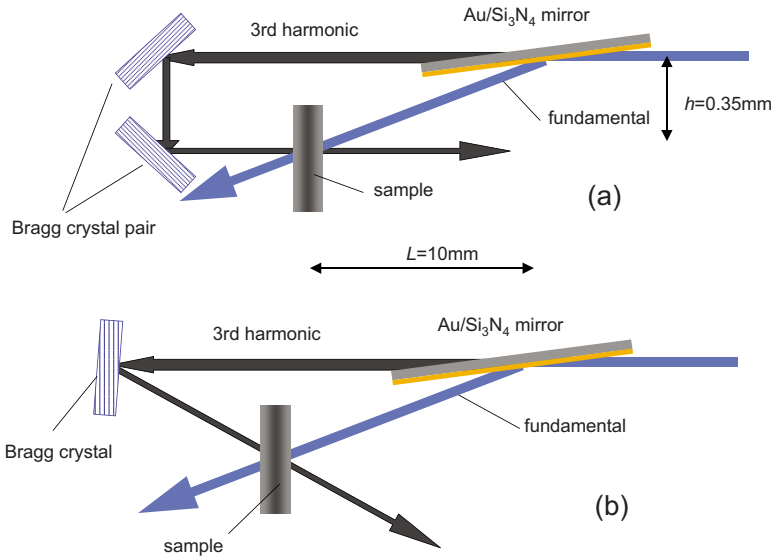

FIG. 8. (Color online) Schematic of possible pump-probe systems using Bragg crystals. Once the Bragg angle is determined by the choice of crystal and wavelength of the XFEL, the distance between the crystals sets the target-crystal distance and thus the overall delay. In both (a) and (b) the grazing-incidence mirror operates at 1° and reflects half of the fundamental. For a 20 nm Au layer and 15 nm Si_3N_4 layer, the transmission of the fundamental is 70%.

photons per shot. In order to resolve the scatter spectral profiles well, we would need to implement a crystal spectrometer. For the third harmonic wavelength regime (1.33 Å) typical crystals include quartz (21–31) with $2d=3.082$ Å. This crystal, for example, is available as a spherical crystal with a radius of 150 mm. In second order, it would be practical to have a spectrum extending 0.5 keV, allowing the Compton profiles from the L and M shells to be collected. With a collection efficiency of 10^{-4} sr we would clearly need of order 100–1000 shots to gather sufficient signal. At $T\sim 10$ eV the foil itself would generate insignificant numbers of emission photons in this regime even for first-order reflection from the crystal at ~4.7 keV.

The experimental layout proposed in Ref. [34] requires pointing accuracy of better than 50 μrad (the beam divergence would be ~3 μrad) for 100 fs delay between pump and probe, with increasing accuracy required for longer delays. As discussed above, this is so soon after heating that it is likely that the melting of the lattice to form a plasma should take longer than this.

An alternative that has been proposed in discussion of the first experiments [35] is to use Bragg crystals as shown in Fig. 8. Two possible arrangements are illustrated schematically. An unfocused beam will have a diameter of ~65 μm [5]. With a 4-mm-length Au mirror on a Si_3N_4 substrate, we can reflect the fundamental at a glancing angle of 1° onto the target. This will allow $>10^{15}$ W cm^{-2} incident flux, allowing heating of our Al slab to a few eV [34] without focusing. The third harmonic passes to either a single crystal or a pair of crystals—the choice of crystal would be coordinated with fine tuning of the XFEL to achieve the required Bragg reflection condition. Bragg crystals can have a high peak reflectivity but a typical rocking curve has a width of $\sim 10^{-4}$ rad; with a bandwidth of $\sim(1-3)\times 10^{-3}$ we expect to reflect of the order of 10% of the third harmonic energy back to the sample, thus increasing the numbers of shots needed to above 1000. Since the energy absorbed by the mirror is likely to be of order ~1 J cm^{-2}, the mirror will be damaged by each shot. However, micrometer-accuracy motion control can be used to move a new surface of the mirror into the beam easily enough for a 10 Hz shot rate. Likewise, both the crystal and a target foil can be moved to present a new surface to each shot.

Referring to Fig. 8, if we assume, for example, that the mirror-sample distance $L=10$ mm, then the offset $h=0.35$ mm; enough to allow the third harmonic beam to pass. The delay between the fundamental and third harmonic then depends on the distance to (and between) the Bragg crystals. For millimeter-scale targets we expect delays in the range 10–50 ps to be possible. This is long enough for melting of the crystal structure to a plasma to occur. In Fig. 9 we see that a 1 μm foil heated by a 10^{15} W cm^{-2} beam at 3.1 keV is still very uniform and close to solid density at 10 ps delay. By reducing the heating; and thus expansion, or by using a slightly thicker foil we can even improve on this. These delays are long enough for melting of the lattice to form a plasma structure, and the issue of a modestly heated foil changing from a crystal to a plasma structure [23] can be explored by observing the angularly and spectrally resolved scatter as a function of delay with this scheme.

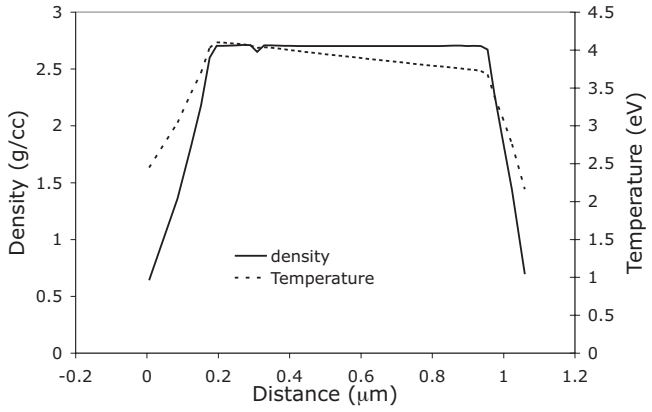

FIG. 9. Density and temperature profiles of a 1 μm Al foil, 10 ps after heating with a 3.1 keV XFEL pulse at 10^{15} W cm^{-2}, simulated with the HYADES hydrodynamics code [36] using the SESAME tabular equation of state to link pressure to density and temperature [37].

Since the bandwidth of the XFEL beam is of order 10^{-3}, the pointing of the beam onto the crystal has to be good to ~ 1 mrad. This is a somewhat looser constraint than the pointing for the double-mirror scheme and, although still technically challenging in the details, we believe the scheme would be feasible and worth some effort to achieve.

V. SUMMARY

We have presented calculations of the scatter spectra that might be expected from an XFEL-heated slab of warm dense matter. We have particularly concerned ourselves with making new calculations of the bound-free Compton profiles, specifically for a dense plasma environment. These give us access to the outer electron wave functions, which are themselves central to the bulk behavior of the material, i.e., the equation of state.

ACKNOWLEDGMENTS

This work was supported by EPSRC Grant No. EP/D031532/1. G.S.N. was supported by the Higher Education Commission of Pakistan Grant No. 8-1/S-PAEC/HEC/2004/25.

[1] Committee on High Energy Density Plasma Physics, Plasma Science Committee, National Research Council, chaired by R. C. Davidson, *Frontiers in High Energy Density Physics—the X-games of Contemporary Science* (National Academies Press, Washington, DC, 2003).
[2] Committee on Physics of the Universe, Board of Physics and Astronomy, National Research Council of the National Academies, chaired by M. S. Turner, *Connecting Quarks with the Cosmos: Eleven Science Questions for the New Century* (National Academies Press, Washington, DC, 2003).
[3] *Compton Scattering*, edited by B. Williams (McGraw-Hill International, London, 1977).
[4] P. M. Platzmann, P. Eisenberger, and N. Tzoar, in *Proceedings of the Second International Conference on Light Scattering in Solids*, edited by M. Balkanski (Flammarion Sciences, Paris, 1971).
[5] TESLA Technical Design Report Supplement, DESY Report No. DESY2002-167, TESLA-FEL 2002-09, edited by R. Brinkmann, B. Faatz, K. Flottmann, J. Rossbach, J. R. Schneider, H. Schulte Schrepping, D. Trines, Th. Tschentscher, and H. Weise, 2002 (unpublished), DESY Library, Notkestrasse 85, D-22603 Hamburg, Germany.
[6] R. W. Lee, H. A. Baldi, R. C. Cauble, O. L. Landen, J. S. Wark, A. Ng, S. J. Rose, C. Lewis, D. Riley, J. C. Gauthier, and P. Audebert, Laser Part. Beams **20**, 527 (2002).
[7] R. W. Lee, S. J. Moon, H. K. Chung, W. Rozmus, H. A. Baldis, G. Gregori, R. C. Cauble, O. L. Landen, J. S. Wark, A. Ng, S. J. Rose, C. L. S. Lewis, D. Riley, J. C. Gauthier, and P. Audebert, J. Opt. Soc. Am. B **20**, 770 (2003).
[8] S. H. Glenzer, G. Gregori, R. W. Lee, F. J. Rogers, S. W. Pollaine, and O. L. Landen, Phys. Rev. Lett. **90**, 175002 (2003).
[9] S. H. Glenzer, O. L. Landen, P. Neumayer, R. W. Lee, K. Widmann, S. W. Pollaine, R. J. Wallace, G. Gregori, A. Höll, T. Bornath, R. Thiele, V. Schwarz, W.-D. Kraeft, and R. Redmer, Phys. Rev. Lett. **98**, 065002 (2007).
[10] O. L. Landen, S. H. Glenzer, M. J. Edwards, R. W. Lee, G. W. Collins, R. C. Cauble, W. W. Hsing, and B. A. Hammel, J. Quant. Spectrosc. Radiat. Transf. **71**, 465 (2001).
[11] G. Gregori, S. H. Glenzer, and O. L. Landen, J. Phys. A **36**, 5971 (2003).
[12] A. Höll, R. Redmer, G. Röpke, and H. Reinholz, Eur. Phys. J. D **29**, 159 (2004).
[13] J. Chihara, J. Phys.: Condens. Matter **12**, 231 (2000).
[14] G. Gregori, A. Ravasio, A. Höll, S. H. Glenzer, and S. J. Rose, High Energy Density Phys. **3**, 99 (2007).
[15] P. Holm and R. Ribberfors, Phys. Rev. A **40**, 6251 (1989).
[16] B. Bloch and L. B. Mendelsohn, Phys. Rev. A **12**, 1197 (1975).
[17] B. Bloch and L. B. Mendelsohn, Phys. Rev. A **12**, 551 (1976).
[18] M. Schumacher, F. Smend, and I. Borchert, J. Phys. B **8**, 1428 (1975).
[19] D. A. Liberman, J. Quant. Spectrosc. Radiat. Transf. **27**(3), 335 (1982).
[20] W. R. Johnson, C. Guet, and G. F. Bertsch, J. Quant. Spectrosc. Radiat. Transf. **99**, 327 (2006).
[21] G. Gregori, S. H. Glenzer, and O. L. Landen, Phys. Rev. E **74**, 026402 (2006).
[22] S. Ichimaru, *Basic Principles of Plasma Physics* (Addison-Wesley, Reading, MA, 1973).
[23] S. Mazevet, J. Clerouin, V. Recoules, P. M. Anglade, and G. Zerah, Phys. Rev. Lett. **95**, 085002 (2005).
[24] O. Peyrusse, J. Quant. Spectrosc. Radiat. Transf. **99**, 469 (2006).
[25] B. F. Rozsnyai, Phys. Rev. A **5**, 1137 (1972): The original expression includes a multiplicative factor α that reproduces the exact Hartree-Fock exchange energy as well as possible. Here we take Slater's original 2/3, but for condensed phases it is usually taken to be 1. However, we found the results are not very sensitive to the value of α.
[26] R. M. More, Adv. At. Mol. Phys. **21**, 305 (1985).
[27] D. B. Boercker and R. M. More, Phys. Rev. A **33**, 1859 (1986).
[28] M. S. Daw and M. I. Baskes, Phys. Rev. B **29**, 6443 (1984).
[29] R. Kubo, J. Phys. Soc. Jpn. **12**, 570 (1957).
[30] D. Pines and P. Nozieres, *The Theory of Quantum Liquids* (Perseus Books, Cambridge, MA, 1999).
[31] R. Redmer, H. Reinholz, G. Röpke, R. Thiele, and A. Höll, IEEE Trans. Plasma Sci. **33**, 77 (2005).
[32] P. Eisenberger and P. M. Platzman, Phys. Rev. A **2**, 415 (1970).
[33] A. Krenz and J. Meyer-ter-Vehn, Eur. Phys. J. D **36**, 199 (2005).
[34] J. J. Angulo Gareta and D. Riley, High energy density physics **2**, 83 (2006).
[35] R. W. Lee *et al.*, http://www-ssrl.slac.stanford.edu/lcls/papers/
[36] J. T. Larsen and S. M. Lane, J. Quant. Spectrosc. Radiat. Transf. **51**, 179 (1994).
[37] Los Alamos National Laboratory report No. LA-UR-92–3407, edited by S. P. Lyon and J. D. Johnson (1992), see http://t1web.lanl.gov/doc/SESAME_3Ddatabase_1992.html